The Scientific Journal of University of Benghazi

SJUOB (2023) 36 (2) Applied Sciences: 104 – 111

Melad et al

http://journals.uob.edu.ly/sjuob

Parametric Study and Optimization the Effect of TIG Welding Process Parameters on the Corrosion Resistance of 2205 DSS Weldment using Potentiodynamic Polarization Technique

Mohamed S. Melad [1]*, Mohamed A. Gebril [1], Farag M. Shuaeib [1], Farag I. Haidar [1], Dawod M. Elabar [1], Salah M. Elkoum [2]

1 Mechanical Engineering Department- Faculty of Engineering- University of Benghazi.

2 The great man- made river

Received 19/ 10 / 2023; Accepted 09 / 11 / 2023

الملخص

الهدف من هذه الدراسة هو تحليل تأثير عوامل لحام القوس الكهربائي والغاز الخامل وهي تيار اللحام وسرعة اللحام وكمية غاز النتروجين المضافة مع الأرغون كغاز حماية على مقاومة التآكل لوصلات لحام الفولاذ المزدوج الطور المقاوم للصدى والحصول على أفضل قيم لهذه العوامل باستخدام الطريقة الاحصائية لتصميم التجارب (منهجية الاستجابة السطحية) لغرض تقليل معدل التآكل. يمتلك الفولاذ المقاوم للصدأ على خصائص ميكانيكية عالية ومقاومة جيدة للتآكل نظرا لاحتوائه على خليط من عناصر السبك التي تجعله يمتلك بنية مجهرية مزدوجة ومتساوية بين طور الاوستينايت وطور الفرايت. مشكلة الفولاذ المقاوم للصدأ مزدوج الطور هي ان في اغلب تطبيقاته يحتاج لعملية لحام وعملية اللحام تسبب في تغير البنية المجهرية وتكوين ترسبات في منطقة اللحام التي تؤدي الى ضعف الخصائص الميكانيكية ومقامة التآكل. ولذلك من المهم التحقق من تأثير عوامل اللحام على مقامة التآكل لوصلات لحام الفولاذ المقاوم للصدأ مزدوج الطور. في هذه الدراسة , تم استخدام التقنية الكهروكيميائية (استقطاب الجهد) لحساب معدل التآكل لجميع وصلات لحام الفولاذ المزدوج الطور. تم استخدام ايضا الطريقة الاحصائية (منهجية الاستجابة السطحية) لغرض الحصول على نموذج رياضي يوصف العلاقة بين العوامل المذكورة مسبقا ومعدل التآكل لوصلة لحام الفولاذ المزدوج الطور. النتائج الاحصائية اظهرت ان تيار اللحام واضافة غاز النتروجين مع الارغون كغاز حماية هما أكثر عاملين مؤثرين على مقاومة التآكل لوصلات لحام الفولاذ المزدوج الطور. كذلك تبين أن زيادة تيار اللحام مع إبطاء سرعة اللحام أدى إلى زيادة معدل التآكل نتيجة ظهور ترسبات. من ناحية أخرى تناقص تيار اللحام مع زيادة سرعة اللحام الذي يدل على أقل كمية حرارة ادى ايضا الى زيادة معدل التآكل نتيجة لزيادة كمية طور الفرايت. تبين من خلال النتائج ايضا ان اضافة كمية قليلة من غاز النتروجين مع الارغون كغاز حماية يؤدي الى تقليل معدل التآكل. من ناحية أخرى، زيادة كمية غاز النتروجين مع غاز الارغون يؤدي ايضا الى زيادة معدل التآكل نتيجة لإعادة ظهور الترسبات.

الكلمات المفتاحية: الفولاذ المقاوم للصدأ مزدوج الطور، عملية لحام القوس الكهربائي والغاز الخامل، غاز النيتروجين كغاز حماية، منهجية الاستجابة السطحية، التقنية الكهروكيميائية لاستقطاب الجهد.

Abstract

The aim of this research is to analyze and optimize, using response surface methodology RSM, the effect of tungsten inert gas TIG welding parameters, namely welding current WC, welding speed WS, and N_2 addition with Ar as shielding gas, on the corrosion resistance of duplex stainless steel DSS weldments. Due to the combination of alloying elements and the nearly equal amounts of austenite and ferrite phases, DSS has great mechanical characteristics and good corrosion resistance. However, most DSS applications require welding processes to join parts together; these processes affect the microstructure of DSS and lead to the formation of precipitations, resulting in poor mechanical properties and corrosion resistance. Therefore, it is necessary to investigate the effect of TIG welding process parameters on the corrosion resistance of DSS weldments. In this study, the corrosion penetration rate of all DSS weldments was determined using the potentiodynamic polarization technique. The response surface methodology was applied in order to achieve the mathematical model that describes the relationship between above mentioned welding variables and corrosion penetration rate of DSS weldment. Results showed that WC and N_2 are the most important parameters that affected the corrosion penetration rate. Meanwhile, the results clarified that when increasing WC with decreasing WS, which corresponds to the highest heat input, the corrosion penetration rate increased due to the appearance of the precipitations. The same results were obtained for decreasing welding current while increasing welding speed, which corresponds to the lowest heat input due to the increase in ferrite content. On the other hand, the results also found that the addition of a small amount of N_2 with Ar as shielding gas leads to a decrease in the corrosion penetration rate. However, the increase in the amount of N_2 leads to an increase in the corrosion penetration rate due to the reappearance of the precipitations.

Keywords: Duplex stainless steel, TIG welding process, N_2 as shielding gas, Response surface method, potentiodynamic polarization technique.

***Correspondence**: Mohamed S. Melad

Mohamed.almalki@uob.edu.ly

1. INTRODUCTION

The most popular type of austenitic-ferritic steels, also known as duplex stainless steel DSS, contain a combined microstructure of austenite and ferrite and are utilized in a variety of applications. They offer greater levels of strength than austenitic steels and are appropriate for a variety of corrosive environments. Although they have high ductility, DSSs have less formability than austenitics due to their higher strength. They are easily welded and have superior stress corrosion cracking resistance [1,2].

Particularly in applications where the double yield strength may be used in the design to reduce the wall thickness, duplex alloys can be lower-cost substitutes for austenitic grades with equivalent corrosion resistance. In pressure vessel and storage tank applications where weight reduction through reduced wall thickness decreases the cost of material, welding, and transportation, duplex stainless steels are successfully used [3]. The extensive use of stainless steel duplexes as a riser pipe in the Man-Made River Project in Libya is due to their percentage of ferrite and austenite phases and the amount of alloying elements, these combined benefits made this material had superior strength and corrosion resistance as well as a good welding capacity. But when the fusion welding process carried out this percentage will be disturbed, and then the superior properties will be lost. In another word, variations in hardness, a reduction in tensile strength, and a loss of corrosion resistance would all detrimentally affect the characteristics of the region around the weld-bead heat-affected zone HAZ [2]. I. J. Moon et al. [4] established the relationship between the sigma phase precipitation and microstructural change as well as the resistance to pitting corrosion of a super duplex stainless steel (UNS S32750) weld formed using a tungsten inert gas TIG welding technique. They reached the conclusion that a slow cooling rate caused sigma phase precipitation to form in weld metal, whereas a comparatively fast cooling rate did not allow a sigma phase to precipitate. Xue-fang Xie et al. [5] examined the use of the multi-pass welding method for the microstructure characterization of DSS weldments. After conducting testing, they concluded that there was a significant phase imbalance at the weld fillers and HAZ; the austenite was dominating at the weld fillers, whereas ferritiszation occurred at the HAZ. Additionally, they found that the austenitic phase morphologies varied at different welding zones, with more intergranular forming at the WM and lathy grain boundary austenite and small Widmanstätten austenite detected at the HAZ. These phenomena are related to the multipass welding's reheating cycles, which might negatively affect the DSS's desirable qualities, including toughness and corrosion resistance. The passivity of stainless steels is strongly influenced by nitrogen, one of the alloying elements of DSS, and it is beneficial to increase the DSS's resistance to pitting corrosion, pit propagation, crevice corrosion, intergranular corrosion, and stress corrosion cracks [6-10]. The duplex grades contain up to 0.4% nitrogen to provide better austenite phase development while welding because nitrogen promotes the initial stage of austenite phase formation at higher temperatures throughout the weld cooling cycle [8]. It has been reported that weldments of nitrogen-containing duplex stainless steels suffer pitting attacks as a result of nitrogen loss because certain amounts of the nitrogen that is present in the DSS may be lost during welding [9]. Z. Zhang et al. [10] compared the attributes of the precipitations of Cr2N and γ2, such as the corrosion resistance of DSS, utilizing the TIG welding procedure. They concluded that the N2-supplemented shielding gas significantly improved austenite formation and decreased the tendency for Cr2N precipitation in the HAZ. A. Topić and N. Knezović [11] studied the effect of N2 addition with Ar as shielding gas on the mechanical properties of 2 mm thickness 2205 DSS produced with laser welding process. After tests, they found that the shielding gas mixture type obviously does not have a significant influence on ultimate tensile strength. Furthermore, they said that the used of N2 in shielding gas should be researched further and should include impact toughness and pitting corrosion resistance testing, which would give even more reliable guidelines for ferrite amount. A. R. Pimenta et al. [12] studied how much N2 should be added to the shielding gas to create an autogenous TIG joint in a hyper DSS. They stated that a nearly linear relationship could be seen between the volume portion of austenite in the weld metal and the increase in nitrogen content. A. Baghdadchi et al. [13] investigated effects of N2 addition as shielding gas using autogenous laser welding and reheating in welding of 1.5 mm-thick DSS. They concluded that the welded austenite fraction increased from 22 to 39% when changing the shielding and backing gas from pure argon to pure nitrogen. Moreover, they found that the laser reheating increased the austenite fraction from 39 to 57% for the N2-shielded weld, while there were no any measurable effects when using Ar shielding. However, they also observed some nitrides in WM and HAZ for both Ar and N2 shielding, but the amount was lower with N2 shielding.

The mechanical properties of DSS weldments are directly influenced by the changes in TIG welding parameters and this is clarified by G. Ghadi and S. Shivakumar [14] when doing research employing TIG welding process parameters on mechanical properties of 6 mm thickness austenitic stainless steel weld joint. The mechanical properties obtained by mechanical testing are analyzed with input process parameters using design of experiments technique. They concluded that the high welding current and high inert gas flow rate with lower diameter of the filler wire give maximum tensile strength. Moreover, they found that the low welding current and lower diameter with higher inert gas flow rate give maximum bending strength. On the other hand, R. S. Vidyarthy et al. [15] studied the influence of Activated-TIG welding process parameters such as welding current, welding speed and flux coating density on different aspects weld bead geometry of ferritic stainless steel FSS. Using response surface methodology, the depth of penetration and depth to width ratio were investigated and optimized. After tests, they found that the optimized depth of penetration and depth to width ration of 6.95 mm and 0.80, respectively, were obtained at the welding current of 213.78A, welding speed of 96.22 mm/min, and the flux coating density of 1.99 mg/cm2. Moreover, they stated that the Welding current is the most significant input variable affecting weld bead geometry of FSS. Thabet M. Elrabei and Ezzeddin. M. Anawa [16] examined the impacts of several TIG welding process input parameters on the ultimate tensile strength and micro-hardness of 3 mm-thick austenitic stainless steel using the Taguchi technique. After conducting tests, they stated that the welding speed is the factor that has the biggest effect on the tensile strength and micro-hardness of the weld joint. Additionally, they found that the highest ultimate tensile strength and maximum micro-hardness obtained at the same level of welding current of 140 A, welding speed of 190 mm/min, and gas flow rate of 4 L/min are 641.67 MPa and 202.5 HV, respectively. However, for the same problem of this study and to determine the ideal welding setting, Ibrahem. Z, et al. [17] studied a TIG welding technique on duplex stainless steel material 2205 with a 6mm thickness. They discovered, using the Taguchi approach, that the ideal welding current, welding speed, and gas flow rate were 198.19 A, 146.121 mm/min, and 7 l/min, respectively. The responses provided results of ultimate tensile strength of 1068.842 MPa, hardness of 46.996 HRD, and impact of 91.776 J. The authors concentrated on the mechanical characteristics of the DSS weld joint, but upon microstructure inspection, they noticed some Cr precipitation on the grain boundary, which led them to emphasize the importance of further research into corrosion resistance of DSS. S. Mondal et al. [18] determined the optimal process conditions for TIG welding of DSS to achieve the desired weld mechanical properties. Grey-based Taguchi methodology for process optimization has been carried out to solve this multi-response optimization problem. After that, an ANOVA test has been carried out to identify the significance of the individual factor on the desired responses. They found that the optimal welding parameters were welding current 90A, gas flow rate 8 L/min, and welding speed 3.5 mm/s, which obtained the highest yield and ultimate tensile strength. Furthermore, they also concluded that the most significant factor was welding speed.

In summary, to improve the corrosion resistance of DSS weldments, it is important to control the parameters of TIG welding process that directly influenced the heat input using design of experiment DOE. However, many authors showed that the addition of N2 with Ar as shielding gas has a beneficial effect on the corrosion resistance of DSS weldments and no any work was found for the effect of the N2 gas amount by DOE method. Therefore, The present study aimed to exploit advantages of applying group of TIG welding process experiments using response surface methodology, and carry out these experiments on DSS samples in order to determine the optimum TIG welding parameters and N2 amount that minimize the corrosion penetration rate of DSS weldments.

2. METHODOLOGY

2.1 Material and Welding Process

The work material for the experiments in this study was duplex stainless steel DSS 2205 (UNS S32205). Preparing for welding, the base metal was cut into plates measuring 6.35x140x100 mm using an abrasive water jet cutting machine. The TIG welding machine that is used in this process is known as a DWHP250NL. The constant arc gap was 2 mm, and the tungsten electrode utilized had a 2.4 mm diameter and an 8 mm cup size. ER2209, which has a 1.6 mm thickness, was the filler material used in this investigation. Table 1 displays the chemical composition of the base metal and the ER2209 filler material. Figure 1 depicts the schematic diagram of the welding procedure.

Table 1. Chemical composition of DSS and ER2209 filler material

Component	Cr	Ni	Mn	C	Si	P	Mo	N	Fe
Base Metal Wt%	22.2	4.70	1.72	0.03	0.037	0.03	2.55	0.17	Balance
Filler Material (wt%)	23	8.5	1.6	0.02	0.5	>0.01	3.1	0.11	Balance

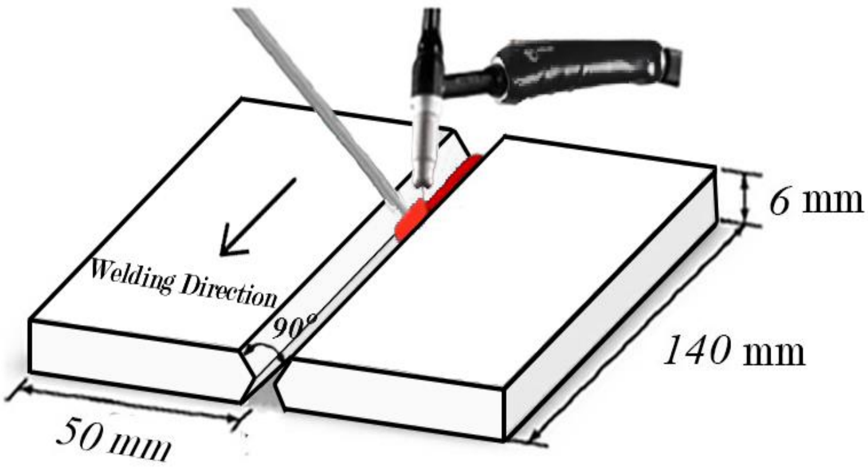

Fig 1. Schematic diagram of the welding process

2.2 Response Surface Methodology

Response Surface Method RSM has been adopted for planning the experiments of welding duplex stainless steel. The experimental design matrix was developed as per the central composite rotatable design (CCD) of RSM. Three factors were varied at five levels, resulting in a rotatable CCD matrix consisting of 8 cube points, 6 center points in the cube, and 6 axial points. 20 butt-welded samples have been made using five levels of welding current, welding speed, and the amount of N2 added to Ar as shielding gas with a constant flow rate of 10 L/min. The response measured is the corrosion penetration rate.

The optimization and prediction of the response were carried out using the response surface design technique. Based on the trial runs and literature review, the levels of the factors are determined and exhibited in Table 2. After setting up and introducing the factorial levels for each input variable into a MINITAB_19 program, we get the input experiment matrix for the welding processes. Table 3 demonstrates the matrix of welding process experiments and the resultant corrosion rate of each design point.

Table 2. The range values of welding process variables

No.	Input Parameter	Levels				
		-2	-1	0	1	2
1	Welding current (A)	140	155	170	185	200
2	Welding speed (mm/min)	135	155	175	195	215
3	N_2 (%)	0	5	10	15	20

2.3 Microstructure Characterization

The water jet cutting machine was used to cut the weld joint samples from the original DSS weldment. The microstructure of the samples with high and low corrosion rates was examined using an OLYMPUS BX61 optical microscope and an EP50 digital camera in order to clarify and illustrate the results. The samples were ground and polished in accordance with the ASTM-E407-2002 standard (ground using silicon carbide abrasive sheets), using grit sizes ranging from 240 to 1200 and water as lubricant and coolant. The samples are cleaned with water, then polished with diamond paste and cooling oil using 3 mm and 1 mm billiard cloth to provide a smooth, mirror-like finish on the sample surfaces. The samples were then dipped in 1 g of K2S2O5, 15 mL of HCL, and 85 mL of distilled water for Beraha's etching solution.

2.4 Corrosion Test

The original DSS weld joints were cut into rectangular samples for the corrosion tests, which were then connected to an electric wire mounted with epoxy to expose a uniform area. After that, the samples were mechanically ground with SiC emery paper up to 800 grits, rinsed with distilled water, and quickly dried in hot air. Electrochemical polarization measurements were performed using the ACM instrument field machine potentiostat in conjunction with a saturated Ag/AgCl reference electrode and graphite counter electrode. In order to ensure that the Ecorr becomes constant, the samples were immersed in 3.5% sodium chloride (simulating sea water) for 20 hours under open circuit conditions. After that, the cyclic polarization tests were run at a scan rate of 60 mV/min with a swept range of about 500 mV below Ecorr in the anodic direction. When the voltage reached 700 mV, the scanning direction changed upside down. Four readings were taken in each instance to verify that the results would be consistent.

3. RESULT AND DISCUSSION

3.1 Analysis of Corrosion Penetration Rate CPR Performance

Corrosion penetration rate CPR is the rate of metal loss during a chemical or electrochemical reaction with the environment. Changes in welding settings have a direct impact on the rate of corrosion of DSS weld joints. Therefore, it is essential to develop a mathematical model that demonstrates the relationship between the welding parameters and the corrosion rate of DSS weldments. Table 3 contains the completed design matrix with the corrosion rate results.

Table 3 design points matrix and corrosion rate results

No	Input Parameters			Response
	welding current (A)	welding speed (mm/min)	N_2 (%)	CPR (mm/y)
1	185	155	15	0.042736
2	170	175	10	0.020430
3	200	175	10	0.026282
4	155	195	15	0.067919
5	170	175	0	0.046800
6	170	215	10	0.062500
7	170	175	10	0.014000
8	170	175	10	0.010900
9	140	175	10	0.062820
10	170	175	10	0.022500
11	170	175	10	0.028862
12	185	195	5	0.035000
13	185	195	15	0.017100
14	170	175	20	0.029774
15	185	155	5	0.060485
16	155	195	5	0.067428
17	170	135	10	0.103000
18	170	175	10	0.007786
19	155	155	15	0.026109
20	155	155	5	0.050856

3.2 Microstructure Characterization

Figure 2 (a and b), which illustrates the microstructure of the design points 18 and 17 (in Table 3) that, respectively, exhibit low and high CPR. The design point number 17 with high CPR has an austenite volume fraction of 64.6%, whereas the design point number 18 with low CPR has an austenite volume fraction of 56.2%. It is obvious that design point number 17 certainly has a large concentration of Cr2N precipitations as shown in Figure 2(b). On the other hand, Figure 2(a) that shows the microstructure of design point number 18 illustrated that no Cr2N precipitations have been identified. Therefore, the very high austenite concentration and the appearance of Cr2N precipitations are the primary contributors to the decreased CPR in DSS weldments.

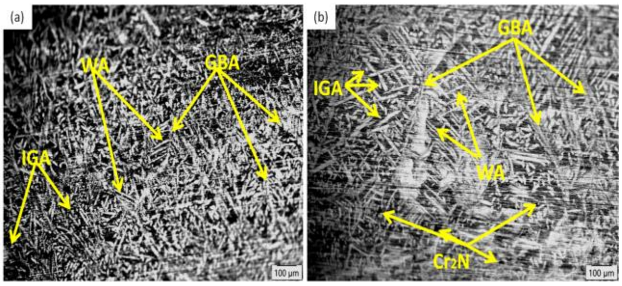

Fig 2. Weld zone microstructure: (a) design point 18, (b) design point 17

3.3 Analysis of Variance ANOVA for Corrosion Penetration Rate

Table 4 shows the analysis results for reduced quadratic model, which is modified by reduced terms based on P value for the calculated corrosion rate. As is generally accepted in statistics, the significance of a model term is indicated if the P-value is less than 0.05. Furthermore, if the P-value is higher than 0.1000, the model term is not considered significant. Additionally, a high F value for a parameter indicates that the parameter has a significant impact on the properties of the weld joint. The results of model analysis showed that the WC, N2, WC×WC, WS×WS, N2×N2, and WC×WS are significant model terms. From Table 4, it can be noted that the highest F value is at a WC of about 12.28, while for welding speed and N2 are equal to 3.95 and 6.41 respectively, which means that welding speed and N2 addition to Ar as shielding gas parameters have less effect on the process. The P value of the WC is 0.004, whereas the WS and N2 are 0.07 and 0.026 respectively. This is indicating that the WC and N2 parameters are significant, but the most significant parameter is WC. Other model adequacy measures R-sq and Adjusted R-sq are presented in the Table 4. The determining factor R-sq indicates the goodness of fit of the model. The value of R-sq of this model is 91.04%. This implies that at least 91.04% of the variability in the data for the response is explained by the model. This indicates that the proposed model is passable.

Table 4 Analysis of variance for corrosion penetration rate results

Source	DF	Adj SS	Adj MS	F-Value	P-Value	
Model	7	0.010494	0.001499	17.41	0.000	Significant
WC (A)	1	0.001057	0.001057	12.28	0.004	
WS (mm/min)	1	0.00034	0.00034	3.95	0.07	
N_2 (%)	1	0.000552	0.000552	6.41	0.026	
WC×WC	1	0.001164	0.001164	13.51	0.003	
WS×WS	1	0.006724	0.006724	78.08	0.000	
N_2×N_2	1	0.00069	0.00069	8.01	0.015	
WC×WS	1	0.001499	0.001499	17.41	0.001	
Error	12	0.001033	0.000086			
Lack of Fit	7	0.00072	0.000103	1.65	0.302	
Pure Error	5	0.000313	0.000063			
Total	19	0.011527				
R-sq=91.04%			**R-sq(Adj)=85.81%**			

3.4 Mathematical Model of Corrosion Penetration Rate

Linear, square, and interaction regression analyses have been used to develop CPR's mathematical model. It is essential to note that each parameter utilized in this mathematical model must be within the acceptable range shown in Table 2. The welding current (WC), welding speed (WS), and nitrogen addition (N2) process variables have been used to formulate the mathematical equation for CPR:

$$CPR = 0.951 - 0.00284 \times WC - 0.00678 \times WS - 0.00536 \times N_2 + 0.00003 \times WC^2 + 0.000041 \times WS^2 + 0.000209 \times {N_2}^2 - 0.000046 \times WC \times WS$$

Where

Corrosion Penetration Rate CPR in (mmy^{-1})

Welding current WC in (A)

Welding speed WS in (mm/min)

N_2 in (%)

3.5 3D Surface and Contour Plots of Corrosion Penetration Rate

The response value for each given combination of any two parameters is predicted using a three-dimensional (3D) surface plot, with the third parameter being held constant. The influence of these combined characteristics is generally significant if the surface plots show a lot of curvature, bend, or undulation. The combined effect is not significant, however, if the response surface plot does not exhibit significant curvature, bend, twist, or undulation. The contour plots are two-dimensional (2D) plots, and each line or contour within represents a constant response line. Figure 3 (a and b) illustrates the 3D surface and contour plots, respectively, of the effect of the change in WC and WS at a constant middle amount of N2 on the behavior of CPR. From Figure 3(a), the 3D surface plot clearly showed that the lowest CPR can be exhibited at high WC with an approximately middle value of WS. Meanwhile, the highest CPR is obtained when the WC decreases with an increase in WS. Moreover, the contour plot shown in Figure 3(b) performed the same behavior: increasing the WC more than 180A with an increase in WS of 170 mm/min can decrease the CPR by 0.03 mmy-1. The reason can be explained by heat input. Since the increase in heat input leads to an increase in the austenite volume fraction, which subsequently decreases the CPR, However, very high heat input contributes to the appearance of the Cr2N precipitations that have a negative effect on the corrosion resistance of DSS weldments. Therefore, the highest value of WC with an approximately middle value of WS performed an appropriate heat input that led to a decrease in the CPR of DSS weld joints.

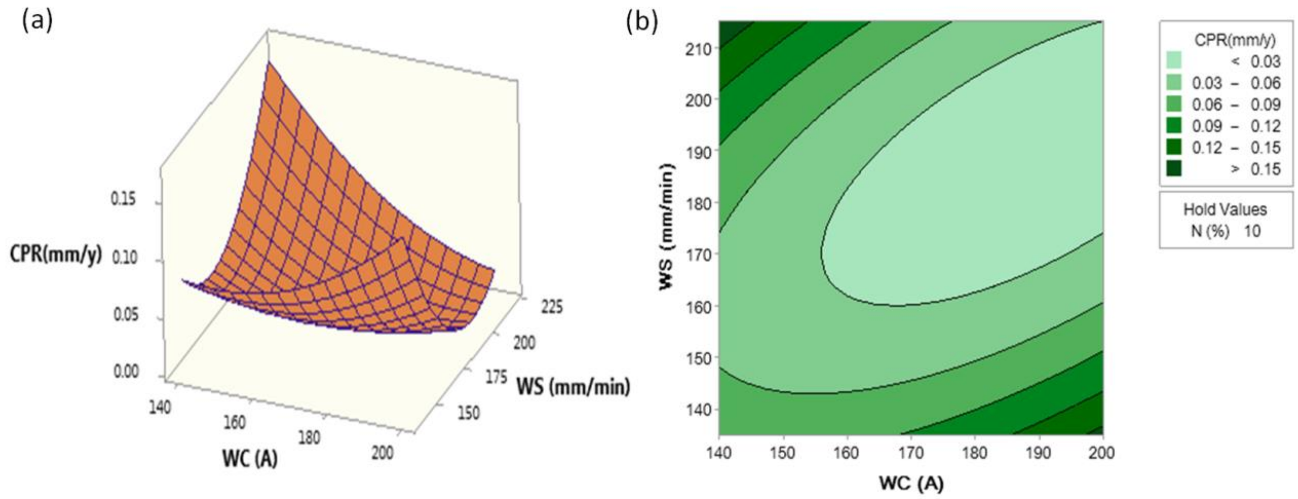

Fig 3. CPR behavior versus WC and WS at constant N2: (a) 3D surface, (b) contour plots

Figure 4 (a and b) demonstrates the effect of the change in WC and N2 addition to Ar as shielding gas at constant WS on the behavior of CPR as a 3D surface and contour plots, respectively. From the 3D surface plot shown in Figure 4(a), it can be seen that at approximately 10% N2, the CPR decreases with an increase in WC up to 190A. However, more than 190A showed an increase in CPR. On the other hand, the contour plot that is illustrated in Figure 4(b) confirmed the same behavior: the lowest CPR can be obtained when the WC ranges from 170 to 190A with the addition of approximately 8 to 18% N2 with Ar as shielding gas. The increase in WC leads to an increase in heat input and an increase in austenite content, which subsequently decreases the CPR. Moreover, the addition of N2 with Ar as a shielding gas also contributes to the increase in austenite content. However, a very high percentage of N2 showed a decreasing trend in the CPR, mainly due to the reappearance of Cr2N precipitations.

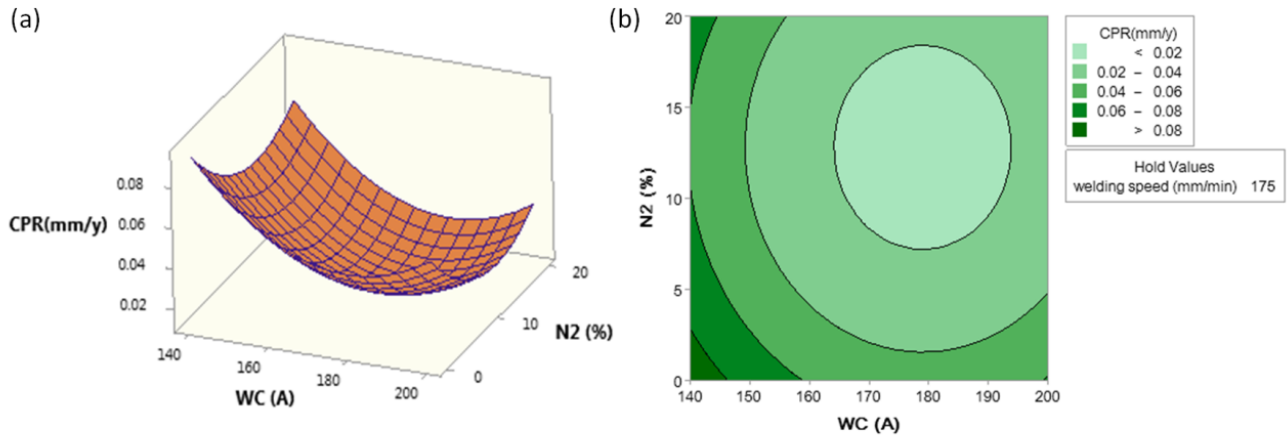

Fig 4. CPR behavior versus WC and N2 at constant WS: (a) 3D surface plot, (b) contour plot

Figure 5 (a and b) represents, respectively, the 3D surface and contour plots of the CPR behavior with the change in WS and N2 addition with Ar as shielding gas at constant WC. The 3D surface plot shown in Figure 5(a) clearly explains that the WS is more influenced than N2 on the CPR; at approximately 10% N2, the CPR decreases with an increase in WS up to 175 mm/min. However, increasing the WS by more than 175 mm/min showed an increasing trend in the CPR. Moreover, from the contour plot that is illustrated in Figure 5(b), the lowest CPR can be obtained from the WS range of 170 to 190 mm/min and N2 addition between 10 and 15%.

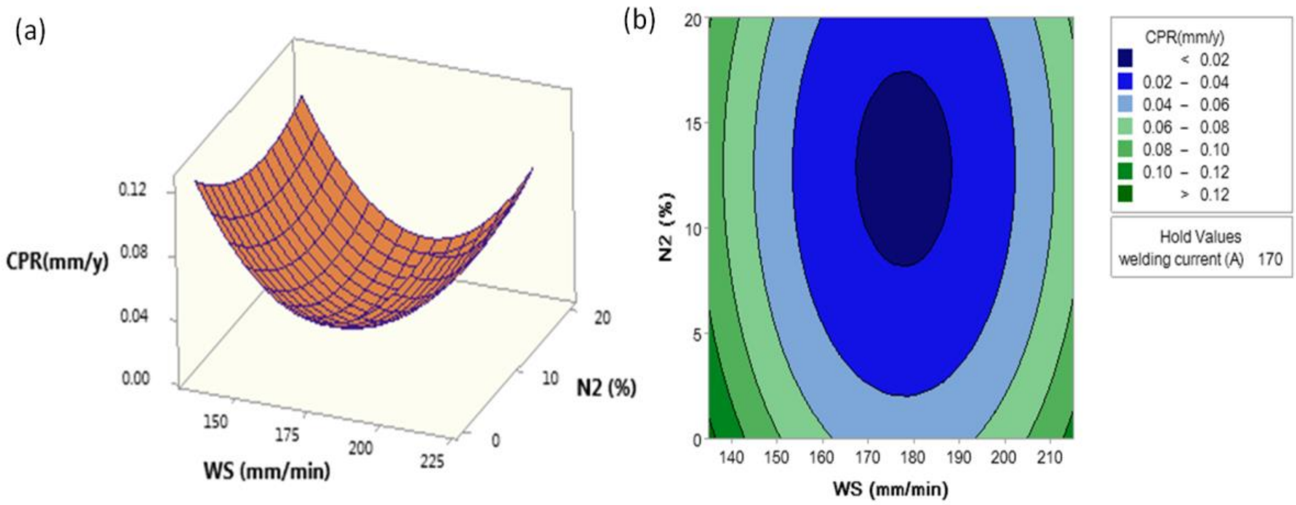

Fig 5 CPR behavior versus WS and N2 at constant WC: (a) 3D surface plot, (b) contour plot

3.6 The Corrosion Penetration Rate Optimization

Figure 6 shows the optimization plot that illustrates the effect of each parameter, namely WC, WS, and N2 addition to Ar as shielding gas, on the CPR of the DSS weldments. In general, the red perpendicular lines on the plot reflect how the parameters have been set, and the red values in parentheses at the top of each column show the numerical values of the ideal parameter (welding) setting. The ideal welding parameter of the corrosion penetration rate response is represented by the blue dashed line and blue numerical value. The goodness-of-fit of this model (D = 0.98642) explained how the selected welding settings satisfy the CPR optimum and work well to reduce CPR. According to Figure 6, the ideal WC, WS, and N2 addition are 190A, 189mm/min, and 13%, respectively, providing a CPR of 0.0091 mmy-1. Furthermore, the model demonstrated with excellent detail how adding a small quantity of N2 and using an appropriate heat input to achieve high austenite content with minimal Cr2N precipitation results in superior resistance to corrosion of DSS weldments.

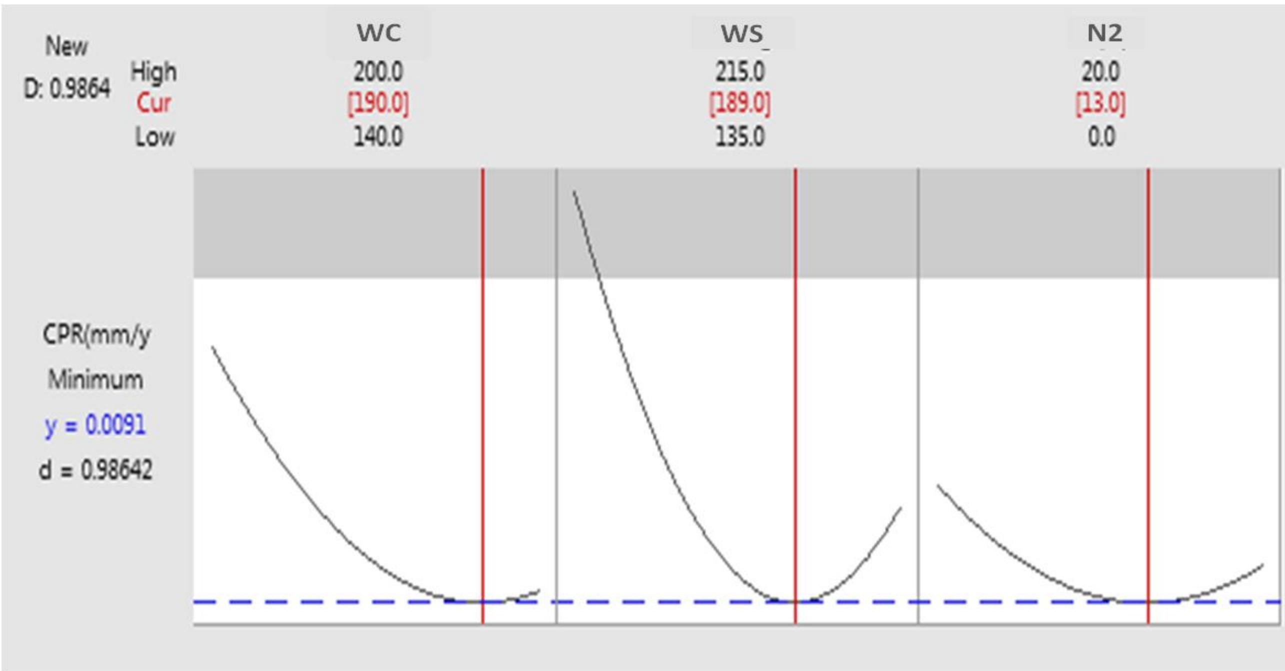

Fig 6. Optimization plot of the WC, WS, and N2 addition to minimize CPR of DSS weld join

4. CONCLUSION

In this study, Response Surface Methodology (RSM) has been used to study the impact of TIG welding settings on the corrosion resistance of duplex stainless steel DSS weld joints. The corrosion resistance of DSS weldments was determined using the potentiodynamic polarization technique and explained by the corrosion penetration rate. The following points summarize the most important outcomes:

1. The RSM results indicated that the corrosion penetration rate is more significantly impacted by the welding parameters WC and N_2.
2. The model correctly predicts the response of the corrosion penetration rate at 91.04%.
3. Due to the presence of precipitation, an increase in WC with a decrease in WS causes a high corrosion penetration rate. However, the same results were achieved when WC was decreased while WS was increased due to an increase in the volume percentage of ferrite.
4. A small amount of N_2 added to argon as a shielding gas improved the corrosion resistance of DSS weld joints by reducing the corrosion penetration rate, whereas adding more N_2 increased the corrosion penetration rate..
5. The RSM results demonstrated that the most effective welding settings (WC=190A, WS=185 mm/min, and N_2 of approximately 13%) result in the lowest corrosion penetration rate (0.0005 mmy^{-1}).

5. REFERENCES

1. Aisc, “Structural Stainless Steel 27 Steel Design Guide,” 2013.
2. K. Y. Benyounis, A. G. Olabi, M. S. Hashmi. Multi-response optimization of CO2 laser-welding process of austenitic stainless steel. Optics & Laser Technology. 2008; 40(1):76-87.
3. E. M. Westin, Welds in the lean duplex stainless steel LDX 2101: effect of microstructure and weld oxides on corrosion properties. (Doctoral dissertation 2008, KTH). https://www.divaportal.org/smash/record.jsf?pid=diva2%3A54604&dswid=-4664
4. I. J. Moon, B. S. Jang, And J. H. Koh, “Heat Treatment Effect on Pitting Corrosion of Super Duplex Stainless Steel Uns S32750 TIG Welds,” In Advanced Materials Research, 2013, Vol. 746, pp. 467–472.
5. Xue-fang Xie, Jingwen Li, Wenchun Jiang, Zhilong Dong, Shan-Tung Tu, Xiangnan Zhai, Xu Zhao ., “Nonhomogeneous Microstructure Formation and its Role on Tensile and Fatigue Performance of Duplex Stainless Steel 2205 Multi-Pass Weld Joints,” Mater. Sci. Eng. A, Vol. 786, P. 139426, 2020.
6. H. Tsuge, Y. Tarutani, And T. Kudo, “The Effect of Nitrogen on the Localized Corrosion Resistance of Duplex Stainless Steel Simulated Weldments,” Corrosion, Vol. 44, No. 5, pp. 305–314, 1988.
7. M. Liljas and R. Qvarfort, “Influence of Nitrogen on Weldments in Vns S 31803,” in Duplex Stainless Steels’ 86. International Conference, 1986, pp. 244–256.
8. T. Ogawa and T. Koseki, “Effect of Composition Profiles on Metallurgy and Corrosion Behavior of Duplex Stainless Steel Weld Metals,” Weld. J., Vol. 68, No. 5, P. 181, 1989.
9. T.-S. Chern, K.-H. Tseng, And H.-L. Tsai, “Study of The Characteristics of Duplex Stainless Steel Activated Tungsten Inert Gas Welds,” Mater. & Des., Vol. 32, No. 1, pp. 255–263, 2011.
10. Z. Zhang, H. Jing, L. Xu, Y. Han, And L. Zhao, “Investigation on Microstructure Evolution and Properties of Duplex Stainless Steel Joint Multi-Pass Welded by Using Different Methods,” Mater. Des., Vol. 109, pp. 670–685, 2016, Doi: 10.1016/J.Matdes.2016.07.110.
11. A. Topić and N. Knezović, International Symposium on Intelligent Manufacturing and Automation, "Influence of Shielding Gas Mixture Type on Ultimate Tensile Strength of Laser-Welded Joints in Duplex Stainless Steel 2205", 2020, Doi: 10.2507/31st.Daaam.Proceedings.Xxx.
12. A. R. Pimenta, M. G. Diniz, G. Perez, And I. G. Solórzano-Naranjo, “Nitrogen Addition to the Shielding Gas for Welding Hyper-Duplex Stainless Steel,” Soldag. E Insp., Vol. 25, pp. 1–8, 2020.
13. A. Baghdadchi, V. A. Hosseini, K. Hurtig, And L. Karlsson, “Promoting Austenite Formation in Laser Welding of Duplex Stainless Steel—Impact of Shielding Gas and Laser Reheating,” Weld. World, Vol. 65, No. 3, pp. 499–511, 2021.
14. G. Ghadi and S. Shivakumar, “Analysis of TIG Welding Process Parameters for Stainless Steel (Ss202),” Int. J. Adv. Eng. Res. Sci., Vol. 3, No. 10, P. 236871, 2016.
15. R. S. Vidyarthy, D. K. Dwivedi, And V. Muthukumaran, “Optimization of A-TIG Process Parameters Using Response Surface Methodology,” Mater. Manuf. Process., Vol. 33, No. 7, pp. 709–717, 2018.
16. Thabet M. Elrabei and Ezzeddin. M. Anawa “Study the Effect of Autogeneous Semiautomatic TIG Welding Process Parameters on Mechanical Properties of Aisi304l Austenitic Stainless steel Using Taguchi Method" , 2019.
17. Ibrahem. Z, Ezzeddin. M. Anawa, Farag. M. Shauieb,. “Controlling and Modelling TIG Welding of Duplex Stainless Steel Using Taguchi Method,” University of Benghazi, 2019.
18. S. Mondal, P. K. Pal, And G. Nandi, “Optimization of Process Parameters of TIG Welding of Duplex Stainless Steel Without Filler Rod by Grey-Taguchi Method,” Indian J. Eng. Mater. Sci., Vol. 28, No. 4, pp. 385–392, 2021.